Spontaneous directional flow of active magnetic particles

Amir Nourhani [1,2,3,4,5,*] and David Saintillan [6,†]

[1]*Department of Mechanical Engineering, University of Akron, Akron, Ohio 44325, USA*
[2]*Department of Biology, University of Akron, Akron, Ohio 44325, USA*
[3]*Department of Mathematics, University of Akron, Akron, Ohio 44325, USA*
[4]*Department of Chemical, Biomolecular, and Corrosion Engineering, University of Akron, Akron, Ohio 44325, USA*
[5]*Biomimicry Research and Innovation Center, University of Akron, Akron, Ohio 44325, USA*
[6]*Department of Mechanical and Aerospace Engineering, University of California San Diego, La Jolla, California 92093, USA*

We predict the emergence of large-scale polar order and spontaneous directional flows in a class of self-propelled autonomous particles that interact via passive repulsion between off-center sites. The coupling of active motion with the passive torque acting about the particle centers results in hybrid active–passive interactions responsible for a macroscopic phase transition from an isotropic state to a polar-aligned state in systems of particles with front interaction sites. We employ a continuum kinetic theory to explain that the emergence of long-ranged orientational order, which occurs in unbounded domains at finite densities, can be externally activated independently of the self-propulsion mechanism and drives a macroscopic particle flow in a direction selected by symmetry breaking.

Self-organization and collective motion are hallmarks of soft active matter [1,2], from dense bacterial suspensions [3,4] to biopolymer and motor-protein solutions [5–8] to colloidal swimmers [9–11], rollers [12–14], and spinners [15–17]. These phenomena, which derive from activity-driven interparticle interactions, often take the form of chaotic spatiotemporal patterns [18,19] as in bacterial turbulence [4] or of cluster formation by motility-induced phase separation [20]. As a result, these systems typically suffer from strong spatial heterogeneity, also known as giant number fluctuations, and rarely display large-scale directional flow, other than in confined geometries [21–26].

In this Letter we introduce a class of self-propelled autonomous particles with off-centered repulsive interaction sites. Suspensions of such particles are capable of macroscopic self-organization with system-size orientational order and directional flow as well as damped concentration fluctuations. An isotropic-to-polar phase transition occurs in unbounded domains in the absence of guiding walls such that the resulting macroscopic flow direction is self-selected by symmetry breaking. These emergent dynamics are not only of fundamental interest in nonequilibrium statistical physics, but also for the design of active colloidal swarms capable of performing controllable collective tasks in practical applications.

The off-centered interaction sites carried by the particles can be either located away from (rear-site) or toward (front-site) the direction of motion. As we demonstrate here, hybrid active–passive interactions emerge from the coupling of active

self-propulsion with the passive torque acting about the particle centers. In the case of rear-site particles, Nourhani *et al.* [27] showed that these hybrid interactions cause an effective attraction of passively repulsive particles leading to contactless particle aggregation. Our focus here is on suspensions of front-site particles, which display radically different collective behavior, and on elucidating their emergent macroscale dynamics.

The mechanism for self-propulsion is irrelevant to the present discussion, as long as the swimmers are autonomous, i.e., their direction of motion is not controlled by any external field but is set solely through interparticle interactions.
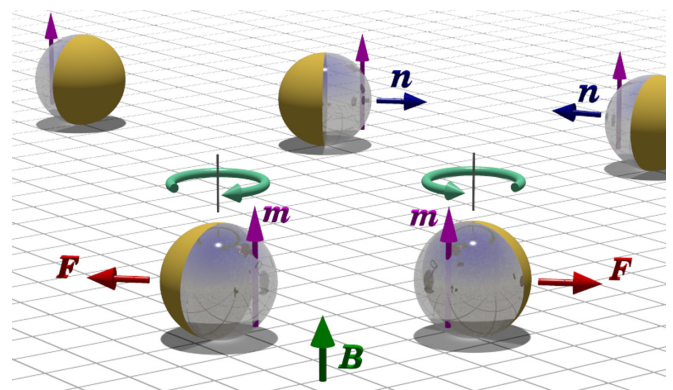

FIG. 1. System schematic: autonomous self-propelled spherical colloids with active velocity $\boldsymbol{v}_s = v_s \boldsymbol{n}$ move on a two-dimensional substrate and interact via off-centered interaction sites, e.g., magnetic moments $\boldsymbol{m}$. An external magnetic field $\boldsymbol{B}$ aligns the moments perpendicular to the plane of motion. Pair interactions between moments lead to both forces and torques about the particle centers.

*nourhani@uakron.edu
†dstn@ucsd.edu

An experimentally realizable system of front-site particles is represented in Fig. 1 and consists of spherical Janus colloids that are half coated with a thin magnetic material on the hemisphere pointing in the direction $\boldsymbol{n}$ of active motion. Upon application of a magnetic field $\boldsymbol{B}$ perpendicular to the plane of motion, magnetic moments $\boldsymbol{m}$ (either induced by $\boldsymbol{B}$ or existing permanently inside the magnetic layer) align with $\boldsymbol{B}$ and exert repulsive forces on each other along with torques about the particle centers. The magnetic torques reorient the particles so they turn away from each other, while the active motion causes them to part ways. Therefore, in the case of two swimmers in isolation, these hybrid active–passive interactions tend to repel the particles as well as reorient them in an antiparallel way such that they swim apart, even in the presence of thermal noise.

In a system at finite density, the particles cannot swim away and must instead stay together and cooperate. While repulsive interactions are expected to damp density fluctuations, the net effect of magnetic torques on large-scale behavior is less obvious. On the one hand, the propensity for antiparallel orientations may allow for an isotropic phase. On the other hand, a spatially uniform system reaches its minimum magnetic energy when the particle directors are aligned in a given direction. This hints at the existence of a macroscopic polar phase in which a mean-field restoring magnetic torque competes against orientational noise to maintain alignment.

We study these emergent phenomena within a continuum kinetic theory framework. Our system consists of N identical self-propelled spherical particles of radius a undergoing overdamped planar motion above a flat surface in a fluid of viscosity η and magnetic permeability μ. The area fraction of the particles is $\phi = \pi a^2 N/S$, where S is the total area of the system assumed to occupy a periodic square domain. Each particle is characterized by its position $\boldsymbol{x}$ and unit director $\boldsymbol{n}$, which determines the direction of its active velocity $\boldsymbol{v}_s = v_s \boldsymbol{n}$, with constant magnitude. Each particle carries a magnetic moment $\boldsymbol{m}$ normal to the direction of motion ($\boldsymbol{m} \perp \boldsymbol{n}$) and located at $\boldsymbol{x} + \ell \boldsymbol{n}$, where the magnet offset ℓ has a constant positive value less than the particle radius. The vertical magnetic field only aligns $\boldsymbol{m}$ upward but has no effect on the direction of active motion $\boldsymbol{n}$. The particles also perform Brownian motion with translational and orientational diffusivities $D_t = k_B T/6\pi\eta a$ and $D_o = k_B T/8\pi\eta a^3$, respectively, where $k_B T$ is the thermal energy.

In addition to active and thermal motions, the particles are subject to magnetic interactions, which are repulsive between individual magnets but also induce torques about the particle centers due to the magnet offsets. The force and torque experienced by a particle at $(\boldsymbol{x}, \boldsymbol{n})$ due to the magnet on another particle at $(\boldsymbol{x}', \boldsymbol{n}')$ in a planar configuration are

$$\boldsymbol{F} = \frac{3\mu m^2}{4\pi} \frac{\boldsymbol{R}}{R^5}, \quad \boldsymbol{T} = \ell \boldsymbol{n} \times \boldsymbol{F}, \quad (1)$$

where $\boldsymbol{R} = \boldsymbol{y} + \ell(\boldsymbol{n} - \boldsymbol{n}')$ and $\boldsymbol{y} = \boldsymbol{x} - \boldsymbol{x}'$ are the magnet-to-magnet and center-to-center relative positions, respectively. The resulting linear and angular velocities in the overdamped regime are $\boldsymbol{F}/6\pi\eta a$ and $\boldsymbol{T}/8\pi\eta a^3$, respectively. The interplay of active self-propulsion, magnetic interactions, and Brownian motion is captured by two dimensionless groups: the Péclet number $\mathrm{Pe} = v_s a/D_t$ compares advective

transport due to swimming to translational diffusion, while $\Omega = D_o^{-1}/(32\pi^2\eta a^6/3\mu m^2)$ is the ratio of the timescales for orientational diffusion and magnetic rotations. Equivalently, the product $\Omega \ell/a$ is the characteristic ratio of magnetic and Brownian torques and quantifies the tendency of moment-moment interactions to align the particle directors against thermal orientational noise.

We investigate the system's behavior in the continuum limit, where its configuration is described by the density function $\Psi(\boldsymbol{x}, \boldsymbol{n}, t)$ for finding a particle at $\boldsymbol{x}$ oriented toward $\boldsymbol{n}$ at time t, which integrates to N over the entire system. We also define the local concentration $c(\boldsymbol{x}, t) = \int \Psi \, d\boldsymbol{n}$, local polarization $\boldsymbol{p}(\boldsymbol{x}, t) = c^{-1} \int \Psi \, \boldsymbol{n} \, d\boldsymbol{n}$, and global polarization $\boldsymbol{P}(t) = V^{-1} \int \boldsymbol{p} \, d\boldsymbol{x}$. In the following we use dimensionless variables and scale lengths with a, time with D_o^{-1}, forces with $3\mu m^2/4\pi a^4$, and the density function with N/S. The evolution of the system is governed by the Fokker–Planck equation,

$$\partial_t \Psi + \nabla_{\boldsymbol{x}} \cdot (\dot{\boldsymbol{x}}\Psi) + [(\boldsymbol{I} - \boldsymbol{n}\boldsymbol{n}) \cdot \nabla_{\boldsymbol{n}}] \cdot (\dot{\boldsymbol{n}}\Psi) = 0, \quad (2)$$

with flux velocities $(\dot{\boldsymbol{x}}, \dot{\boldsymbol{n}})$ given by

$$\dot{\boldsymbol{x}} = \tfrac{4}{3}\left(\mathrm{Pe}\,\boldsymbol{n} + \pi^{-1}\phi\,\Omega\,\boldsymbol{F} - \nabla_{\boldsymbol{x}}\ln\Psi\right), \quad (3)$$

$$\dot{\boldsymbol{n}} = (\boldsymbol{I} - \boldsymbol{n}\boldsymbol{n}) \cdot (\pi^{-1}\phi\,\Omega\,\ell\,\boldsymbol{F} - \nabla_{\boldsymbol{n}}\ln\Psi). \quad (4)$$

The magnetic force exerted on a particle at location $\boldsymbol{x}$ with orientation $\boldsymbol{n}$ by the rest of the system is given by

$$\boldsymbol{F}(\boldsymbol{x}, \boldsymbol{n}, t) = \iint_{|\boldsymbol{y}|\geqslant 2} \Psi(\boldsymbol{x}', \boldsymbol{n}', t)\frac{\boldsymbol{R}}{R^5}\, d\boldsymbol{n}' \, d\boldsymbol{x}', \quad (5)$$

where the integral over relative positions omits the excluded volume region $|\boldsymbol{y}| < 2$. Away from high concentrations where $\ell \ll |\boldsymbol{y}|$, we can expand the force (5) in powers of ℓ up to linear order,

$$F_i(\boldsymbol{x}, \boldsymbol{n}, t) = [c \star K_i] + \ell\,[c(n_j - p_j) \star \mathcal{K}_{ji}] + \mathcal{O}(\ell^2), \quad (6)$$

where $[g \star h] = \int g(\boldsymbol{x}')h(\boldsymbol{x} - \boldsymbol{x}')\, d\boldsymbol{x}'$ is the spatial convolution, and where the interaction kernels are $K_i(\boldsymbol{y}) = y_i/|\boldsymbol{y}|^5$ and $\mathcal{K}_{ij}(\boldsymbol{y}) = \partial K_i/\partial y_j$. Note that ϕ and Ω always appear as a product in Eqs. (3) and (4), with $\phi\,\Omega$ describing the mean-field strength of magnetic interactions.

We first simulate the governing equations (2)–(4) and (6) inside a square periodic domain of width L using a pseudospectral method [29], and results are showcased in Fig. 2; also see video in Supplemental Material [28]. The initial condition is given by the uniform isotropic distribution $\Psi_0(\boldsymbol{x}, \boldsymbol{p}) = (2\pi)^{-1}$ perturbed by uncorrelated white noise. Figure 2(a) shows snapshots from two simulations with $\phi\,\Omega = 2.55$ (bottom row) and $\phi\,\Omega = 10.2$ (top row), and all other parameters kept the same ($\ell = 0.75$, $\mathrm{Pe} = 5.0$). At very short times, both cases exhibit random fluctuations with locally polarized patches pointing in random directions that were present in the initial condition. In the first case (weak repulsive interactions), these fluctuations decay and the system rapidly relaxes towards the uniform isotropic state Ψ_0 with uniform concentration $c(\boldsymbol{x}, t) = c_0 = 1$ and zero polarization $\boldsymbol{p}(\boldsymbol{x}, t) = \boldsymbol{0}$. In the second case (strong repulsive interactions), the polarized patches gradually align and merge to reach a uniformly polarized state with the same uniform concentration $c(\boldsymbol{x}, t) = c_0$ but with a finite nonzero polarization $\boldsymbol{p}(\boldsymbol{x}, t) = \boldsymbol{P}_\infty$ with
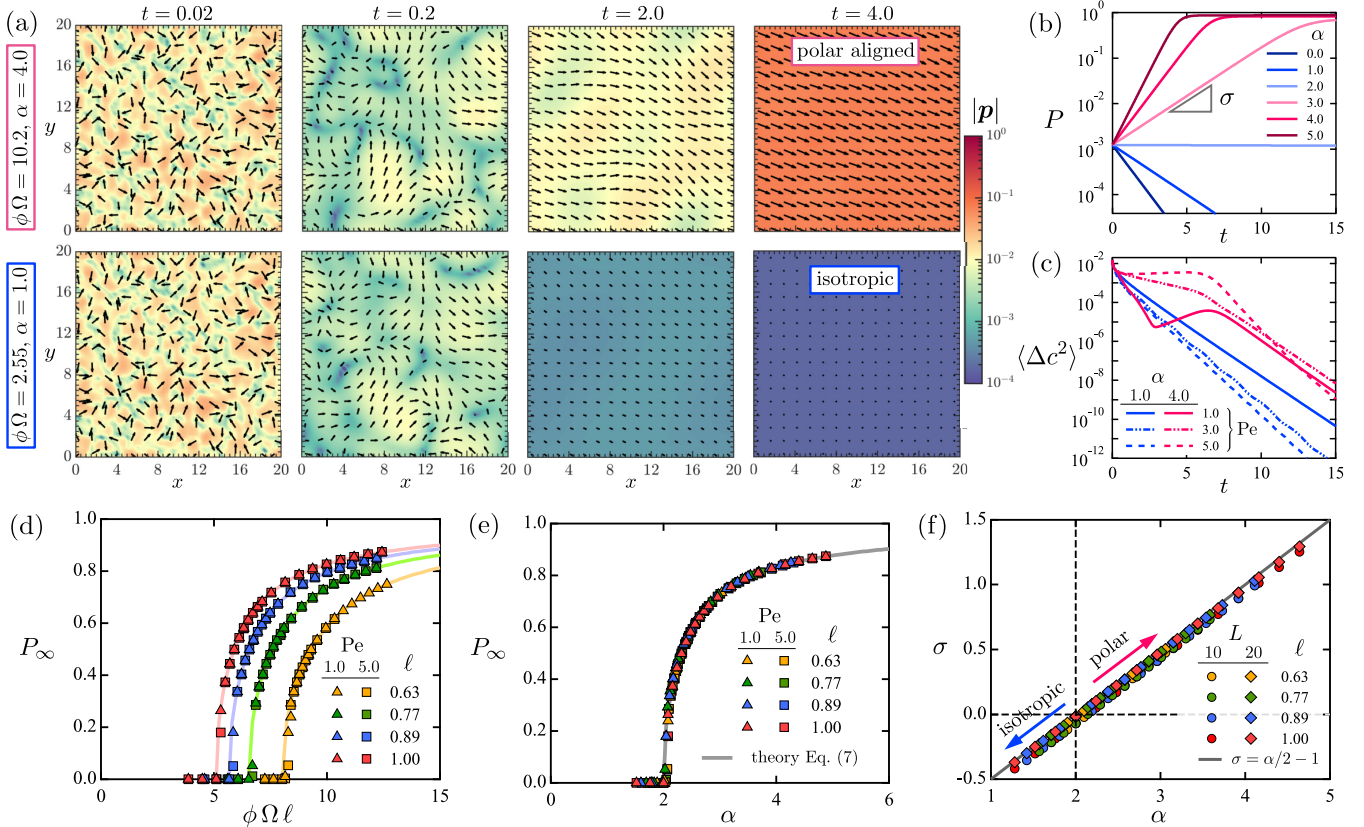
FIG. 2. (a) Snapshots of the polarization field $\boldsymbol{p}(\boldsymbol{x}, t)$ in two-dimensional periodic simulations of Eqs. (2)–(4), starting from a random initial condition in a domain of width $L = 20$ with $\ell = 0.75$ and Pe = 5.0. In this figure, the parameter α is defined as $\alpha = \pi \phi \Omega \ell^2 / 8$. In one case (top row, $\phi \Omega = 10.2$, $\alpha = 4.0$), the system evolves to a uniformly polarized state, whereas in the other case it becomes uniformly isotropic (bottom row, $\phi \Omega = 2.55$, $\alpha = 1.0$). See video in Supplemental Material [28]. (b) Evolution of the global polarization $P(t) = |\boldsymbol{P}(t)|$ in simulations with increasing values of $\phi \Omega$ (or, equivalently, α), with $\ell = 0.75$ and Pe = 5.0. (c) Evolution of the concentration variance $\langle \Delta c^2 \rangle = \langle (c - c_0)^2 \rangle$ for various combinations of α and Pe. (d) Steady-state polarization P_∞ as a function of $\phi \Omega \ell$ for various offset lengths ℓ and Péclet numbers Pe. (e) Steady-state polarization P_∞ as a function of α, showing collapse of all the data with a supercritical pitchfork bifurcation at $\alpha_c = 2.0$. The full curve shows a numerical solution of Eq. (7) for p_0. (f) Growth rate $\sigma = d \ln P / dt$ of the global polarization in simulations for various combinations of system size L and magnet offset ℓ, showing a linear dependence on α in agreement with the linear stability analysis prediction $\sigma = \alpha/2 - 1$.

magnitude $0 < P_\infty < 1$. The direction of $\boldsymbol{P}_\infty$ depends on random fluctuations in the initial condition, since the system is periodic with no preferred direction. This global polarization is accompanied by a net macroscopic particle flow with mean velocity $\boldsymbol{U}_\infty = (4/3) \mathrm{Pe} \, \boldsymbol{P}_\infty$, or $v_s \boldsymbol{P}_\infty$ in dimensional form.

Figure 2(b) shows the evolution of the global polarization $P(t) = |\boldsymbol{P}(t)|$, in simulations with increasing values of $\phi \Omega$, for $\ell = 0.75$ and Pe = 5.0. When $\phi \Omega \lesssim 5.09$, the polarization decreases exponentially towards zero as the system relaxes to isotropy. However, as soon as $\phi \Omega \gtrsim 5.09$, $P(t)$ is found to grow exponentially and ultimately plateau at P_∞, corresponding to the polar aligned state observed in Fig. 2(a). Increasing $\phi \Omega$ results in a larger growth rate $\sigma = d \ln P / dt$ during the transient, as well as in a larger steady-state polarization P_∞.

Irrespective of $\phi \Omega$, the concentration variance $\langle \Delta c^2 \rangle = \langle (c - c_0)^2 \rangle$ is found to decay in Fig. 2(c), with both isotropic and polar systems reaching the uniform concentration $c_0 = 1$ at long times. The decay, however, is found to be slower and nonmonotonic in cases with growing polarization, especially for large values of Pe. Indeed, the transient dynamics in this

case involve the growth and coalescence of polarized patches, resulting in a nonsolenoidal polarization field that drives concentration fluctuations by self-propulsion via a source term of the form $\propto \mathrm{Pe} \nabla_{\boldsymbol{x}} \cdot (c \boldsymbol{p})$ in the evolution equation for $c(\boldsymbol{x}, t)$ [30]. This explains the temporary growth of $\langle \Delta c^2 \rangle$, which decays again once the patches have merged and the polarization nears its global asymptote.

The steady-state polarization P_∞ is plotted versus magnetic torque strength $\phi \Omega \ell$ for various magnet offsets ℓ in Fig. 2(d). For a given ℓ, P_∞ is zero at low values of $\phi \Omega$ but is found to bifurcate, above a given threshold, to a positive value independent of Pe. This indicates a phase transition from the isotropic state to a globally aligned flowing state upon increasing $\phi \Omega$, with a critical threshold that is delayed as the magnet offset decreases. To explain these findings, we first seek an exact steady solution of the Fokker-Planck equation that is spatially uniform but has nonzero polarization: $\Psi = \Psi(\boldsymbol{n})$, with $c = c_0$ and $\boldsymbol{p} = \boldsymbol{p}_0$. In this case the solution is obtained by setting the orientational flux (4) to zero, where the mean-field magnetic force is simply $\boldsymbol{F}(\boldsymbol{n}) = -\pi \ell (\boldsymbol{n} - \boldsymbol{p}_0)/8$. The solution is of the Boltzmann type: $\Psi(\boldsymbol{n}) \propto \exp(\alpha \, \boldsymbol{n} \cdot \boldsymbol{p}_0)$,

where $\alpha = \pi\phi\,\Omega\,\ell^2/8$. Applying the normalization $\int\Psi\,d\boldsymbol{n} = 1$ and polarization $\int\Psi\,\boldsymbol{n}\,d\boldsymbol{n} = \boldsymbol{p}_0$ constraints provides an implicit equation for the magnitude of the polarization:

$$0 = I_1(\alpha p_0) - p_0 I_0(\alpha p_0) = \sum_{k=0}^{\infty}\frac{\alpha^{2k}p_0^{2k+1}}{4k!(k+1)!}\Big[\frac{\alpha}{2}-1-k\Big], \quad (7)$$

where I_0 and I_1 are modified Bessel functions of the first kind. The parameter α appears as the sole dimensionless group controlling the orientation distribution. The behavior of the solution can be gleaned from the series expansion on the right-hand side. For values of $\alpha < 2$, all the coefficients in the series are strictly negative and the only solution is $p_0 = 0$ (isotropic). At $\alpha = 2$, the coefficient of the linear term becomes zero, indicating that $p_0 = 0$ is a multiple root. Finally, when $\alpha > 2$, the first few coefficients in the expansion are positive while the rest are negative. This implies a nonmonotonic behavior with two roots at $p_0 = 0$ and $p_0 > 0$, confirming the existence of a polar aligned state. In the limit of $\alpha \to \infty$, the second root approaches 1, which corresponds to full polarization in the limit of strong magnetic interactions. These observations are summarized in Fig. 2(e), showing p_0 obtained by numerical solution of Eq. (7) along with the simulation data for P_∞ in Fig. 2(d) replotted vs α. A collapse of all the data is observed, with the bifurcation now occurring at $\alpha_c = 2$. A uniform polar state thus exists for $\alpha > \alpha_c$, i.e., $\phi\,\Omega\,\ell^2 > 16/\pi$, which provides a simple criterion in terms of area fraction ϕ, ratio $\Omega\ell$ of magnetic to Brownian torques, and offset length ℓ.

Our simulations with $\alpha > \alpha_c$ never relax to isotropy, suggesting that the uniform isotropic equilibrium state $\Psi_0 = (2\pi)^{-1}$ in fact becomes unstable past the bifurcation. This is confirmed by a linear stability analysis of the Fokker–Planck equation, where we perturb the equilibrium as $\Psi(\boldsymbol{x},\boldsymbol{n},t) = \Psi_0 + \epsilon\widetilde{\Psi}(\boldsymbol{n},\boldsymbol{x},t)$. In the linear regime, the global polarization of the perturbation field $\widetilde{\boldsymbol{P}}(t) = V^{-1}\iint\widetilde{\Psi}\,\boldsymbol{n}\,d\boldsymbol{n}\,d\boldsymbol{x}$ evolves as $\partial_t\widetilde{\boldsymbol{P}} = (\alpha/2 - 1)\widetilde{\boldsymbol{P}}$, indicating exponential behavior with growth rate $\sigma = \alpha/2 - 1$. The uniform isotropic state is therefore linearly stable for $\alpha \leqslant \alpha_c = 2$ and unstable otherwise. This prediction is consistent with

results from our simulations as shown in Fig. 2(f), where we compare the prediction for σ with the numerical growth rate $d\ln P/dt$ extracted from simulations. Excellent agreement is found for a range of magnet offsets. Numerical data for two different system sizes L suggests a weak effect of scale, with the smaller system exhibiting a slightly lower growth rate.

To summarize, we have introduced a class of active particles with off-centered interaction sites capable of large-scale self-organization. We investigated the phase behavior of suspensions of front-site particles using a mean-field kinetic model and demonstrated that unbounded systems with finite density undergo a transition from an isotropic phase to a macroscopically flowing polar phase with damped density fluctuations. The transition occurs by symmetry-breaking with no preferred flow direction and can be activated externally—by creation or removal of off-center magnets by a magnetic field—and independently of self-propulsion. The phenomenology uncovered here shares similarities with classic flocking models such as the Vicsek [31] and flying XY [32] models, and is also reminiscent of other polar active systems such as Quincke rollers [12,13]. However, the mechanism for the phase transition discussed here is fundamentally different and hinges on the subtle coupling of active motion and off-center passive repulsion. While phoretic Janus colloids with a magnetic hemisphere provide a simple experimental realization for active–passive interactions [27], we stress that the underlying physics is more general and is independent of the specific mechanisms for propulsion and repulsion, which could be achieved experimentally in a variety of ways. This remarkable versatility and tunability may provide a unique platform for studying fundamental mechanisms of polar active collective motion, both theoretically and experimentally. Finally, the ability for these particles to self-organize and display controllable large-scale polar order and directional flows also suggests a new paradigm for the design of programmable particle swarms capable of performing collective tasks involving coherent motions.

[1] D. Saintillan and M. J. Shelley, Active suspensions and their nonlinear models, C. R. Phys. **14**, 497 (2013).

[2] M. C. Marchetti, J. F. Joanny, S. Ramaswamy, T. B. Liverpool, J. Prost, M. Rao, and R. A. Simha, Hydrodynamics of soft active matter, Rev. Mod. Phys. **85**, 1143 (2013).

[3] C. Dombrowski, L. Cisneros, S. Chatkaew, R. E. Goldstein, and J. O. Kessler, Self-Concentration and Large-Scale Coherence in Bacterial Dynamics, Phys. Rev. Lett. **93**, 098103 (2004).

[4] J. Dunkel, S. Heidenreich, K. Drescher, H. H. Wensink, M. Bär, and R. E. Goldstein, Fluid Dynamics of Bacterial Turbulence, Phys. Rev. Lett. **110**, 228102 (2013).

[5] F. J. Nédélec, T. Surrey, A. C. Maggs, and S. Leibler, Self-organization of microtubules and motors, Nature (London) **389**, 305 (1997).

[6] V. Schaller, C. Weber, C. Semmrich, E. Frey, and A. R. Bausch, Polar patterns of driven filaments, Nature (London) **467**, 73 (2010).

[7] T. Sanchez, D. Chen, S. DeCamp, M. Heymann, and Z. Dogic, Spontaneous motion in hierarchically assembled active matter, Nature (London) **491**, 431 (2012).

[8] M. J. Shelley, The dynamics of microtubule/motor-protein assemblies in biology and physics, Annu. Rev. Fluid Mech. **48**, 487 (2016).

[9] I. Theurkauff, C. Cottin-Bizonne, J. Palacci, C. Ybert, and L. Bocquet, Dynamic Clustering in Active Colloidal Suspensions with Chemical Signaling, Phys. Rev. Lett. **108**, 268303 (2012).

[10] I. Buttinoni, J. Bialké, F. Kümmel, H. Löwen, C. Bechinger, and T. Speck, Dynamical Clustering and Phase Separation in Suspensions of Self-Propelled Colloidal Particles, Phys. Rev. Lett. **110**, 238301 (2013).

[11] J. Palacci, S. Sacanna, A. P. Steinberg, D. J. Pine, and P. M. Chaikin, Living crystals of light-activated colloidal surfers, Science **339**, 936 (2013).

[12] A. Bricard, J.-B. Caussin, N. Desreumaux, O. Dauchot, and D. Bartolo, Emergence of macroscopic directed motion in populations of motile colloids, Nature (London) **503**, 95 (2013).

[13] A. Bricard, J.-B. Caussin, D. Das, C. Savoie, V. Chikkadi, K. Shitara, O. Chepizhko, F. Peruani, D. Saintillan, and D. Bartolo, Emergent vortices in populations of confined colloidal rollers, Nat. Commun. **6**, 7470 (2015).

[14] H. Karani, G. E. Pradillo, and P. M. Vlahovska, Tuning the Random Walk of Active Colloids: From Individual Run-and-Tumble to Dynamic Clustering, Phys. Rev. Lett. **123**, 208002 (2019).

[15] J. Yan, S. C. Bae, and S. Granick, Rotating crystals of magnetic Janus colloids, Soft Matter **11**, 147 (2015).

[16] G. Kokot, S. Das, R. G. Winkler, G. Gompper, I. S. Aranson, and A. Snezhko, Active turbulence in a gas of self-assembled spinners, Proc. Natl. Acad. Sci. USA **114**, 12870 (2017).

[17] V. Soni, E. S. Bililign, S. Magkikiadou, S. Sacanna, D. Bartolo, M. Shelley, and W. Irvine, The odd free-surface flows of a colloidal chiral fluid, Nat. Phys. **15**, 1188 (2019).

[18] D. Saintillan and M. Shelley, Emergence of coherent structures and large-scale flows in motile suspensions, J. R. Soc. Interface **9**, 571 (2012).

[19] S. P. Thampi, R. Golestanian, and J. M. Teomans, Vorticity, defects and correlations in active turbulence, Philos. Trans. R. Soc. A **372**, 20130366 (2014).

[20] M. E. Cates and J. Tailleur, Motility-induced phase separation, Annu. Rev. Condens. Matter Phys. **6**, 219 (2015).

[21] A. Creppy, F. Plouraboué, O. Praud, X. Druart, S. Cazin, H. Yu, and P. Degond, Symmetry-breaking phase-transitions in highly concentrated semen, J. R. Soc. Interface **13**, 20160575 (2016).

[22] H. Wioland, E. Lushi, and R. E. Goldstein, Directed collective motion of bacteria under channel confinement, New J. Phys. **18**, 075002 (2016).

[23] M. Theillard, R. Alonso-Matilla, and D. Saintillan, Geometric control of active collective motion, Soft Matter **13**, 363 (2017).

[24] K.-T. Wu, J. B. Hishamunda, D. T. N. Chen, S. J. DeCamp, Y.-W. Chang, A. Fernández-Nieves, S. Fraden, and Z. Dogic, Transition from turbulent to coherent flows in confined three-dimensional active fluids, Science **355**, eaal1979 (2017).

[25] S. Chandragiri, A. Doostmohammadi, J. M. Yeomans, and S. P. Thampi, Flow States and Transitions of an Active Nematic in a Three-Dimensional Channel, Phys. Rev. Lett. **125**, 148002 (2020).

[26] M. Varghese, A. Baskaran, M. F. Hagan, and A. Baskaran, Confinement-Induced Self-Pumping in 3D Active Fluids, Phys. Rev. Lett. **125**, 268003 (2020).

[27] A. Nourhani, D. Brown, N. Pletzer, and J. G. Gibbs, Engineering contactless particle-particle interactions in active microswimmers, Adv. Mater. **29**, 1703910 (2017).

[28] See Supplemental Material available at http://link.aps.org/supplemental/10.1103/PhysRevE.103.L040601 for a video of the simulations of Fig. 2(a).

[29] B. Ezhilan, D. Saintillan, and M. J. Shelley, Instabilities and nonlinear dynamics of concentrated active suspensions, Phys. Fluids **25**, 070607 (2013).

[30] D. Saintillan and M. Shelley, Instabilities, pattern formation and mixing in active suspensions, Phys. Fluids **20**, 123304 (2008).

[31] T. Vicsek, A. Czirók, E. Ben-Jacob, I. Cohen, and O. Shochet, Novel Type of Phase Transition in a System of Self-Driven Particles, Phys. Rev. Lett. **75**, 1226 (1995).

[32] F. D. C. Farrell, M. C. Marchetti, D. Marenduzzo, and J. Tailleur, Pattern Formation in Self-Propelled Particles with Density-Dependent Motility, Phys. Rev. Lett. **108**, 248101 (2012).